Journal of Materials Chemistry B

Accepted Manuscript



This is an *Accepted Manuscript*, which has been through the Royal Society of Chemistry peer review process and has been accepted for publication.

Accepted Manuscripts are published online shortly after acceptance, before technical editing, formatting and proof reading. Using this free service, authors can make their results available to the community, in citable form, before we publish the edited article. We will replace this Accepted Manuscript with the edited and formatted Advance Article as soon as it is available.

You can find more information about *Accepted Manuscripts* in the **Information for Authors**.

Please note that technical editing may introduce minor changes to the text and/or graphics, which may alter content. The journal's standard <u>Terms & Conditions</u> and the <u>Ethical guidelines</u> still apply. In no event shall the Royal Society of Chemistry be held responsible for any errors or omissions in this *Accepted Manuscript* or any consequences arising from the use of any information it contains.



Regulation of multifunctional mesoporous core-shell nanoparticles with luminescence and magnetic properties for biomedical applications

Xiaoqing Hu,[†] Mingliang Wang,[‡] Fei Miao,[‡] Jingwei Ma,[†] Hebai Shen,[†] and Nengqin Jia*,[†]

[†] The Education Ministry Key Laboratory of Resource Chemistry and Shanghai Key Laboratory of Rare Earth Functional Materials, Department of Chemistry, College of Life and Environmental Sciences, Shanghai Normal University, Shanghai 200234, China. *E-mail: nqjia@shnu.edu.cn (N. Jia); Tel.: +86 21 64321045; Fax: +86 21 64321833.

[‡]Department of Radiology, Ruijin Hospital, School of Medicine, Shanghai Jiaotong University, Shanghai 200025, China

ABSTRACT: Gd³⁺-based/mesoporous silica-coated multifunctional core-shell (Y,Gd)₂O₃:Eu³⁺@nSiO₂@mSiO₂ nanoparticles (YGO-Bmnc NPs) with red luminescence, paramagnetic and mesoporous properties are developed as a novel nanomedical platform for combined multimodal diagnosis and therapy. 40 nm-sized (Y,Gd)₂O₃:Eu³⁺ (YGO-Ac) nanocore is synthesized by a labor-saving solvothermal method, 20 nm-sized perpendicularly aligned mesoporous silica shell is then successfully coated onto the nanocore through two-step sol-gel process and a highly efficient surfactant removal method (NH₄NO₃/EtOH). The surface area of nanocore

can be increased from 24 m²/g to 562 m²/g after coating mesoporous silica shell without any core-free silica NPs. Light-emitting Eu³⁺ ion is chosen as a model to study the solvothermal mechanism and downconversion/upconversion luminescence properties of nanocore; Y³⁺ is doped into matrix to enhance energy transfer from Gd³⁺ to the doped Eu³⁺. Further investigation of luminescence property of YGO-Bmnc NPs shows that they are good red phosphors with millisecond-lever fluorescence lifetime $(\tau = 2.54 \text{ms}, 612 \text{nm}, {}^5D_0 - {}^7F_2)$. MTT assay reveals low cytotoxicity of the system with IC₅₀ ([Gd]) >1000 µg/mL (6.36 mM). The possibility of using YGO-Bmnc NPs for optical imaging in vitro has been demonstrated. Magnetic resonance imaging (MRI) in vitro exhibits a high r_1 relaxivity of 5.05 mM⁻¹s⁻¹ and low r_2/r_1 ratio of 1.216 (3.0 T) which is much lower than other existing Gd³⁺-based nanoscale contrast agents, manifesting that YGO-Bmnc NPs can be efficient T₁ contrast agents. In light of their good performance in optical-MR imaging and highly ordered mesoporous structure, it is anticipated that they are suitable for combined multimodal diagnosis and therapy, they can load other imaging agents or drugs to provide complementary information from each imaging modality and guide individual treatment. What's more, the mesoporous silica shell can provide a large venue for the effective modification of various functional groups and biotargets with selectivity and specificity.

1. Introduction

Recently, multifunctional nanostructured materials used for multimodal imaging and simultaneous diagnosis and therapy have attracted extensive attention, because a

single technique is usually incapable of providing enough information for precise diagnosis and effective therapy.¹⁻⁵ However, the construction of a multicomponent composite nanostructure involves multistep synthetic procedures, and sometimes requires rigorous synthetic conditions. 6 To facilitate large scale synthesis and functional homogenization, single-phased mesoporous rare-earth (RE) doped gadolinium NPs with luminescence and magnetic properties become one of the most popular options. On the one hand, by doping different light-emitting RE ions (such as Eu³⁺, Tb³⁺, Er³⁺, Yb³⁺/Er³⁺, Yb³⁺/Tm³⁺, Yb³⁺/Ho³⁺) into Gd³⁺-based host matrixes⁷⁻¹⁰ can realize either downconversion or upconversion multicolor emission with long fluorescence lifetime, these probes can provide high sensitivity and resolution of optical imaging, which makes it complementary to macroscopic imaging modalities such as magnetic resonance imaging (MRI), computed tomography (CT) and positron emission tomography (PET). On the other hand, Gd³⁺-based NPs, ¹¹⁻¹⁵ having as many as seven unpaired electrons in its Gd³⁺ core, have been investigated and emerged as potential T₁-weighted MRI contrast agents. In addition, T₁ contrast agent is more desirable than T₂ agent for the accurate high-resolution imaging because the intrinsic dark signal in T₂-weighted MRI can mislead the clinical diagnosis as the signal is often confused with the signals from bleeding, calcification or metal deposits, and the susceptibility artifacts distort the background image. ¹⁶

Nowadays, it has been considered that treatment would be carried out based on individual differences. Through the combination of diagnosis and treatment, we could make use of molecular imaging techniques to guide individual therapy, monitor drug

distribution, and evaluate treatment effect. Single-phased mesoporous RE doped Gd³⁺-based NPs show great potential for simultaneous optical imaging and MRI, however, the low surface area and lack of active functional groups restrict their further applications in drug delivery and treatment. Mesoporous silica is a good coating material because it is relatively biocompatible, resistant to biodegradation and easy to surface functionalization. Meanwhile, their open mesopores can provide convenient transmission channels which offer the large location for accommodation and release of various cargos ranging from chemical drugs to proteins. 17-21 In particular, more intense luminescence with high radiative quantum efficiency can be achieved by coating the surface of doped NPs with non-crystalline or crystalline shell structures, because the coating layer can activate the 'dormant' light-emitting ions near or on the surface of NPs to participate in the luminescence process.²² Furthermore, mesoporous silica shell allows easy access for water molecules to the magnetic center, which significantly improves the water proton relaxation in MRI.²³⁻²⁵ Herein, mesoporous silica coating based core-shell NPs are highly valuable for improving the stability and biocompatibility of nanocore, providing enlarged specific surface area for higher drug/imaging agents-loading capacity, enabling the coupling and labeling of biotargets with selectivity and specificity, truly realizing combined multimodal diagnosis and therapy.

To date, mesoporous silica coating can be divided into two categories based on the NPs are hydrophobic or hydrophilic. The most representative method for preparing hydrophobic NPs is thermal decomposition^{26,27} of metal precursors in organic media

at a high temperature above 240 °C, the as-prepared hydrophobic NPs can be successfully encapsulated into mesoporous silica NPs via reverse-microemulsion method²⁸ or phase transfer approach. ^{17,29,30} The two coating methods consist of two procedures which are different in first step while similar in second step. For first step, reverse-microemulsion method utilizes the hydrolysis of tetraethyl orthosilicate (TEOS) in cyclohexane solution with Igepal CO-520 as surfactant to precoating a nonporous silica layer on the NPs, while phase transfer method uses cetyltrimethyl ammonium bromide (CTAB) as stabilizing surfactant for the transfer of hydrophobic NPs to the aqueous phase. For second step, sol-gel process is exploited to deposit mesoporous silica shell. However, these two common approaches for mesoporous silica coating cannot be applied to hydrophilic NPs that are insoluble in the nonpolar media. In recent years, the sol-gel synthesis of sandwich-structured nanocomposites with hydrophilic nanocore and perpendicularly aligned mesoporous silica shell has been the subject of extensive research, because their orientated and accessible silica mesopores are very conducive to the adsorption and release of large guest objects. 31-33

According to the reports, the 'ideal' size requirements for NPs developed for cancer treatment are between 70 and 200 nm, ^{34,35} however, to the best of our knowledge, there haven't been reports on Gd³⁺-based NPs with particle size smaller than 200 nm and specific surface area larger than 500 m²g⁻¹ so far.

We have previously studied iron oxide³⁶ and manganese oxide³⁷ NPs as MRI contrast agents, herein, by choosing gadolinium oxide (Gd₂O₃) as host matrix, we establish a new kind of multifunctional nanomedical platform with red luminescence,

paramagnetic and mesoporous properties for combined multimodal diagnosis and therapy. The whole synthetic protocol is represented in Scheme 1. Firstly, uniformly sized hydrophilic (Y,Gd)(OH)₃:Eu³⁺ (YGO-A) NPs were synthesized by a one-pot solvothermal method. Secondly, through two-step sol-gel process and a highly efficient surfactant removal method (NH₄NO₃/EtOH), coating of perpendicularly aligned mesoporous silica shell was successfully achieved without core-free silica NPs. Finally, the dried NPs were calcined to endow crystallinity and mesoporous property to nanocore, resulting in well-dispersed (Y,Gd)₂O₃:Eu³⁺@nSiO₂@mSiO₂ (YGO-Bmnc) NPs. Typically, we choose light-emitting Eu³⁺ ion as a model to study the solvothermal mechanism and downconversion/upconversion luminescence properties of nanocore; through doping Y³⁺ into matrix to enhance energy transfer from Gd³⁺ to the doped Eu³⁺. We comprehensively coordinate their luminescence, magnetic and mesoporous properties, their potential use as optical-MR dual-modal imaging agents are also demonstrated. In addition, to distinguish all kinds of prepared core and core-sell NPs, the abbreviations and main differences between separate samples are listed in Table 1.



Scheme 1. Schematic illustration of the synthetic procedures for multifunctional mesoporous core-shell $(Y,Gd)_2O_3$: Eu³⁺@nSiO₂@mSiO₂ (YGO-Bmnc) NPs. Blue balls represent inorganic sources of lanthanide nitrates $Ln(NO_3)_3$ •6H₂O break down into $Ln(OH)_3$, holes in blue balls represent removal of co-surfactant (CTAB/PVP) by calcination.

Table 1. Abbreviations for core and core-shell NPs.

Sample		Differences			
	YGO-A	Using conc. HNO ₃ as catalyst in solvothermal reaction			
Nanocore	YGO-A*	Using FeCl ₃ •6H ₂ O as catalyst in solvothermal reaction			
	YGO-Ac	Calcination of YGO-A NPs			
	YGO-Ac*	Calcination of YGO-A* NPs			
		The volume ratio of ethanol and water in two-step silica coat			
	YGO-Bm	process: 8:1 for first step and 3:4 for second step			
	YGO-Bm ^{8:1}	8:1 for first and second steps			
Core-Shell	YGO-Bmc	Calcination of YGO-Bm NPs			
NPs	YGO-Bmc ^{8:1}	Calcination of YGO-Bm ^{8:1} NPs			
	YGO-Bmn	Extraction of CTAB templates of YGO-Bm NPs by			
		NH ₄ NO ₃ /EtOH mixture			
	YGO-Bmnc	Calcination of YGO-Bmn NPs			

2. Experimental

2.1. Chemicals. Conc. HNO₃ (65%, v/v), cetyltrimethyl ammonium bromide (CTAB), poly(vinylpyrrolidone) (PVP, K30), N,N-Dimethylformamide (DMF), ethanol, tetraethyl orthosilicate (TEOS, $SiO_2 \ge 28.4\%$), ammonia solution (25~28 wt%) and $FeCl_3 \cdot 6H_2O$ ($\ge 99.0\%$) were purchased from Sinopharm Chemical Reagent Co.(China). Y(NO₃)₃ · $6H_2O$ (99.99%, Aladdin), Gd(NO₃)₃ · $6H_2O$ (99.9%, Sigma-Aldrich), Eu(NO₃)₃ · $6H_2O$ (99.9%, Alfa Aesar), ammonium nitrate (95%, J&K) and other chemical reagents of analytical grade were used directly without further purification.

2.2. Synthesis of Single-Phased Mesoporous (Y,Gd)₂O₃:Eu³⁺ (YGO-Ac) Nanocore. Uniformly sized Gd₂O₃ NPs codoped with 5% Y³⁺ and 10% Eu³⁺ were synthesized by a one-pot solvothermal method (in consideration of gadolinium (III) plays an important role in T₁-weighted MRI, we investigated the effect of doping of Y³⁺ less than 30% on the fluorescence intensity of Gd₂O₃: Eu³⁺ NPs). In a typical procedure, 0.019 g (0.05 mmol) of Y(NO₃)₃•6H₂O₃, 0.428 g (0.95 mmol) of of PVP were dissolved in 30 mL of DMF, 40~60 μL of conc. HNO₃ was added with vigorous stirring. The resulting homogenous suspension was transferred to a teflon lined stainless steel autoclave and maintained at 180°C for at least 12 h. After reaction, the white precipitate (Y,Gd)(OH)₃:Eu³⁺ (YGO-A) NPs were collected by centrifugation, washed 3 times with ethanol to remove ions possibly remained in the final products, and dried in a dryer. Mesoporous (Y,Gd)₂O₃:Eu³⁺ (YGO-Ac) NPs were obtained by calcinating the as-prepared YGO-A NPs at 650°C for 2~5 h with a heating rate of 2°C/min. The contrast group catalyzed by 0.0203g (0.075mmol) of FeCl₃•6H₂O³⁸ instead of conc. HNO₃ was also carried out to lucubrate the impact of catalysts on the properties of NPs, other conditions remaining equal, the prepared NPs were designated as YGO-A*/YGO-Ac*.

2.3. Formation of Perpendicularly Aligned Mesoporous Silica Shell Using Two-Step Method. In the first step, the as-prepared YGO-A NPs (50 mg) were treated with an ethanol/water mixture (80/10, v/v) by ultrasonication for 30 min to get rid of any adsorbed impurities. Subsequently, the treated NPs were separated by

centrifugation, and then well dispersed in the same ethanol/water mixture (80/10, v/v) which was alkalized to pH $9\sim10$ with ammonia solution (25 ~28 wt%, 1.5 mL). The resulting solution was insulated in a pre-heated oil bath (70°C) for 10 min under stirring, 32µL of TEOS was then added dropwise to the dispersion. After 5 h, the product was collected by centrifugation, washed 3 times with ethanol. In the second step, the above mentioned product was redispersed in a new ethanol/water mixture (45/60, v/v), followed by the addition of CTAB (0.30 g) and ammonia solution (1.5 mL). The resulting solution was sonicated for another 30 min and insulated in a pre-heated oil bath (70°C) for 10 min under stirring, 128μL of TEOS was then added dropwise to the dispersion. After 5 h, the product was collected by centrifugation, washed 3 times with ethanol, designated as YGO-Bm NPs. In order to demonstrate that the volume ratio of ethanol/water mixture plays a very vital role in constructing of perpendicularly aligned mesoporous silica shell, ethanol/water mixture (80/10, v/v) was taken as solvent for the control group in the whole silica coating process and designated as YGO-Bm^{8:1} NPs.

2.4. Removal of Template. CTAB templates were removed by a highly simple, efficient, mild ion-exchange method.^{39,40} YGO-Bm NPs were redispersed in 20 mL of ethanol containing 60 mg of ammonium nitrate (NH₄NO₃/EtOH mixture), and insulated in oil bath (60°C) for 1 h under stirring, then the NPs was recovered and washed with ethanol. The procedure was repeated 2~3 times to remove CTAB templates completely. Afterward, the dried NPs were calcined at 650°C for 5 h with a heating rate of 2°C/min to endow crystallinity and mesoporous property to nanocore,

resulting in well-dispersed (Y,Gd)₂O₃:Eu³⁺@nSiO₂@mSiO₂ NPs (designated as YGO-Bmnc). For comparison, YGO-Bm and YGO-Bm^{8:1} NPs were calcined at 650°C directly without any treatment, designated as YGO-Bmc and YGO-Bmc^{8:1}, respectively.

2.5. In Vitro Cytotoxicity of YGO-Bmnc NPs Against Cancer and Normal Cells. Human pancreatic cancer cell line (BxPC-3 cells, adherent cancer cells), human myelogenous leukemia cell line (K562 cells, suspension cancer cells) and glomerular mesangial cell line (MC cells, adherent normal cells) were provided by the Institute of Biochemistry and Cell Biology, SIBS, CAS (China). They were grown in RPMI 1640 (Roswell Park Memorial Institute's medium) supplemented with 10% fetal bovine serum (FBS), 1% penicillin/streptomycin and 2.0 g/L NaHCO₃ in 5% CO₂/95% air at 37°C. An inductively coupled plasma atomic emission spectrometer (ICP-AES, VISTA-MPX, Varian) was used to measure concentration of gadolinium atom (designated as [Gd], µg/mL or mM) after all the YGO-Bmnc NPs were completely etched in concentrated nitric acid (65%, v/v). In vitro cytotoxicity of YGO-Bmnc NPs was measured by performing 3-[4,5-dimethylthialzol-2-yl]-2,5-diphenyltetrazolium bromide (MTT, Sigma-Aldrich) assay on these cells. Cells were initially seeded in 96-well plates at 6×10³ cells/well and were grown for 24 h at 37°C. Subsequently, RPMI 1640 solutions containing YGO-Bmnc NPs with various [Gd] were added to the wells and the cells were incubated for 24 h, 48 h and 72 h respectively. Because only living cells can reduce MTT to dark red formazan which can be dissolved in

DMSO and be monitored by the UV-absorbance at 570 nm, cell viability (%) = $[A]_{\text{test}}/[A]_{\text{control}} \times 100\%$, A stands for mean value of optical density at 570 nm (OD₅₇₀).

- **2.6. Optical Imaging In Vitro.** 1 mL of BxPC-3 cells (10⁵ cells) was seeded in quartz-bottom dish for 24 h at 37°C. Before the attached cells were incubated with RPMI 1640 solution containing YGO-Bmnc NPs ([Gd] = 400 μg/mL), the solution was filtered by a 200 nm filter membrane to remove large aggregates and provide a sterile environment. After incubation for 48 h, extracellular free NPs were washed away with phosphate buffer solution (PBS), cells were fixed by 4% paraformaldehyde solution and stained with blue 4′,6-dia-midino-2-phenylindole (DAPI). Finally, the cells were imaged in bright field and under WU (330~385 nm) excitation using an inverted fluorescence microscope (Olympus IX71).
- 2.7. Magnetic Resonance Imaging In Vitro. Magnetic resonance imaging and relaxation time measurements based on [Gd] were performed on a 3.0 T clinical MRI scanner (Signa HDx, GE Medical System) equipped with an eight channel Head Coil. Different concentrations of YGO-Bmnc NPs ([Gd] = 0.06, 0.12, 0.24, 0.48, 0.96 mM) in normal saline with 1% w/v agarose gel were placed in a series of 5 mL tubes. T_1 measurement was performed using the same multi-slice multi-echo sequence with the following parameters: the repetition time/echo time (TR/TE) = 400/20 ms (TI from 200 to 1200 ms). T_2 measurement was carried out similarly to T_1 except for TR/TE = 1000/13, 26, 39, 52, 65, 78, 91, 104 ms. The resulting T_1 and T_2 values were averaged and plotted as 1/T (s⁻¹) versus [Gd] (mM), the slopes of the graphs provided the specific relaxivities (the longitudinal relaxivity T_1 and the transverse relaxivity T_2).

2.8. Characterizations. Morphologies of the samples were inspected using a scanning electron microscope (FE-SEM, Hitachi S-4800) and transmission electron microscope (TEM, JEOL JEM-2100). The size distributions of samples were checked by dynamic light scattering (DLS) technique using Malvern Zetasizer Nano ZS90 instrument. The X-ray diffraction (XRD) was performed on a Rigaku D/max2200VPC diffractometer equipped with Cu-K α radiation ($\lambda = 0.15406$ nm). N₂ adsorption-desorption isotherms were measured at 77 K with a Micromeritics TriStar II 3020 analyzer after activating the samples under vacuum at 100 °C for at least 6 h; the Brunauer-Emmett-Teller (BET) method was utilized to calculate the specific surface areas (S_{BET}), the total pore volumes (Vp) were estimated from the adsorbed amount at a relative pressure P/P_0 of 0.97, and the adsorption average pore widths (4V/A by BET) were used to represent the pore size (Dp); by using the Barrett-Joyner-Halenda (BJH) model, the pore size distributions were derived from the adsorption branches of isotherms. Fourier-transform infrared (FTIR) spectra were gathered on a Nicolet 380 spectrometer from samples in KBr pellets. Downconversion fluorescence properties were investigated by a Cary Eclipse 4000 spectrophotometer equipped with a xenon lamp as the excitation source. The luminescence decay curves were collected on an Edinburgh LFS-920 fluorescence spectrometer using a pulse laser as excitation source. Upconversion fluorescence spectrum was recorded under 800 nm Ti:Sapphire femtosecond laser (Sequoia, Spectra-Physics) excitation, the pulse width and laser power were set to ~ 35 fs and ~ 3.7 mJ, respectively. The magnetization values of the samples were acquired at room temperature with a Lake Shore 7400 vibrating sample magnetometer (VSM) instrument using an applied magnetic field from 0 to 1.6 T.

3. Results and discussion

3.1. Morphology and Formation Mechanism of Single-Phased Mesoporous (Y,Gd)₂O₃:Eu³⁺ (YGO-Ac) Nanocore. Uniformly sized hydrophilic YGO-A NPs were synthesized by a one-pot solvothermal method with lanthanide nitrates Ln (NO₃)₃•6H₂O (Ln=Y³⁺、Gd³⁺、Eu³⁺) as inorganic sources, conc. HNO₃ as catalyst, CTAB/PVP as co-surfactant, and DMF as solvent. Mesoporous YGO-Ac NPs were obtained by calcinating the as-prepared YGO-A NPs at 650°C(Scheme 1). FE-SEM and TEM images reveal that 40 nm YGO-Ac nanocore with spherical shape are uniform and separated from one another (Figure 1a,b). High-resolution TEM (HR-TEM) images of these YGO-Ac NPs show distinct lattice fringe patterns, indicating the highly crystalline nature of the NPs (Figure 1c,d). Selected area electron diffraction (SAED) pattern further reveals that they are polycrystalline (Figure 1e).

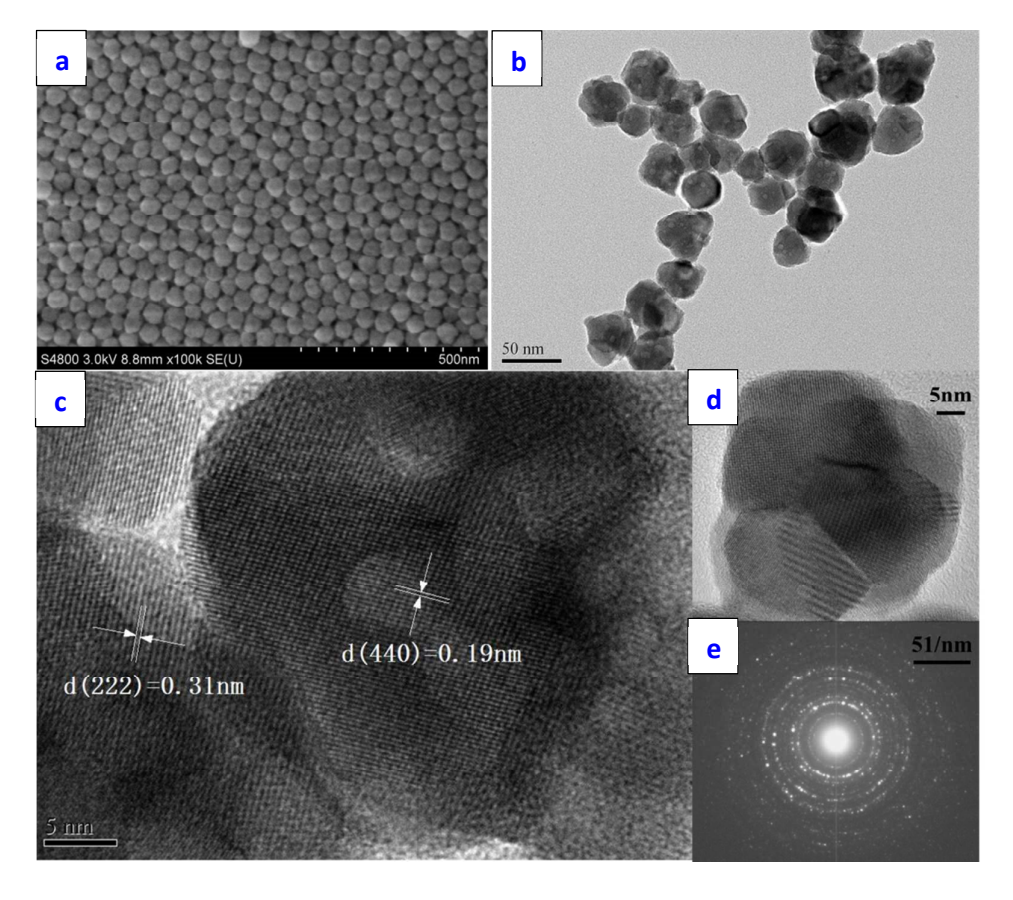


Figure 1. (a) FE-SEM image, (b) TEM image, (c,d) HR-TEM images and (e) selected area electron diffraction (SAED) pattern of monodisperse YGO-Ac NPs.

In the solvothermal process, the nucleation and growth are carefully controlled by co-surfactant and catalyst (Scheme 1). Inorganic sources of lanthanide nitrates Ln(NO₃)₃•6H₂O (Ln=Y³⁺, Gd³⁺, Eu³⁺) break down into Ln(OH)₃ (blue balls) and aggregate into crystal nuclei which are stabilized by the hydrophilic heads of CTAB. When crystal nuclei growing up into nanospheres, PVP coordinates onto their surfaces to prevent them from rapid growth, and the over-protection of PVP to nuclei is avoidable because the carboxyl groups of PVP can interact with positive ionic species, such as CTA⁺ (dissolve from CTAB) and H⁺ (generate from catalyst). The synergistic effects accelerate self-assembly process to produce large scale of uniform

and monodisperse nanospheres.^{38,41} In the process of calcination, the amorphous $Ln(OH)_3$ ($Ln=Y^{3+}$, Gd^{3+} , Eu^{3+}) undergoes two dehydration stages to LnOOH to Ln_2O_3 , and accompanied by removal of co-surfactant, resulting in YGO-Ac NPs with high crystallinity, fluorescence intensity and mesoporous property.

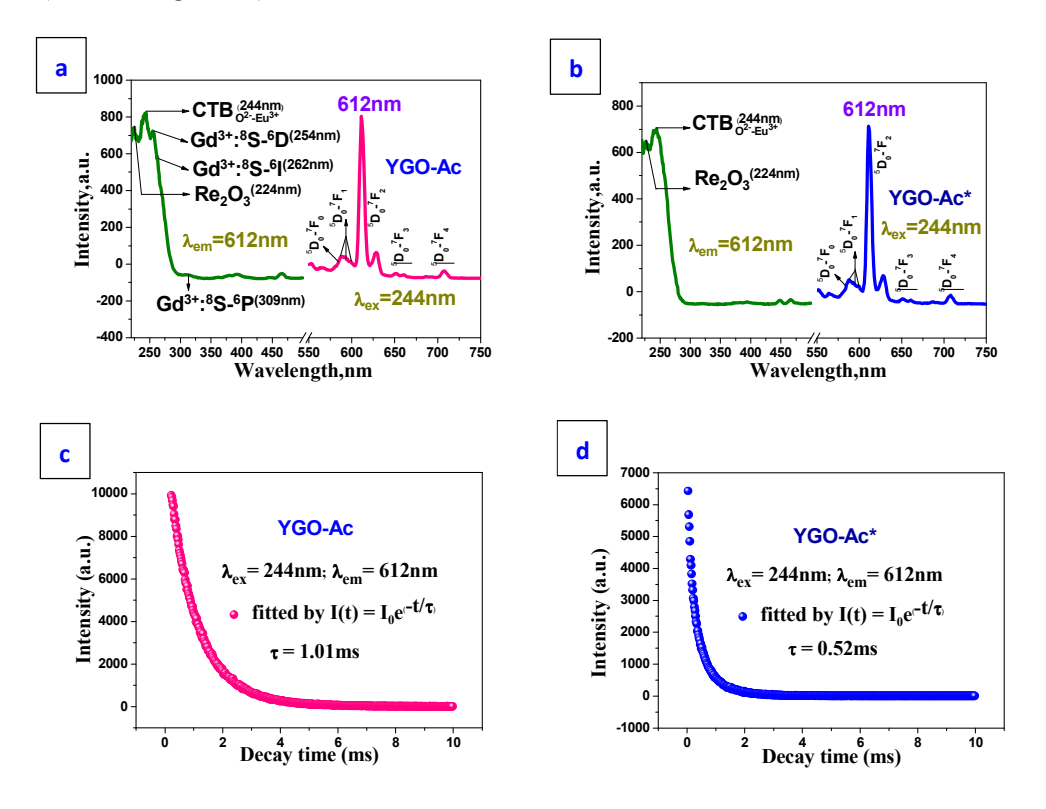
3.2. Functionalities of YGO-Ac NPs Affected by Solvothermal Catalyst Type. We can see sharp contrast in Figure S1, using conc. HNO₃ as solvothermal catalyst will gain a white powder (YGO-A and YGO-Ac NPs) while using FeCl₃•6H₂O as solvothermal catalyst will obtain a brown powder (YGO-A* and YGO-Ac* NPs). However, the two kinds of NPs dispersed in ethanol have similar hydrodynamic size distribution measured by DLS (approximately 60 nm for YGO-A and YGO-A* NPs). The results suggest that the size of NPs mainly depends on the ratio of co-surfactant whereas catalyst type has great impacts on the properties of NPs.

The luminescence properties of NPs affected by two different catalysts were shown in Figure 2a,b. For YGO-Ac NPs catalyzed by conc. HNO₃, the excitation spectrum is mainly composed of a broad intense band (230~280 nm) with a maximum at 244 nm and a weak shoulder at 224 nm due to the charge-transfer band (CTB) between O²⁻~ Eu³⁺ and the (Y,Gd)₂O₃ host excitation band, respectively. The other weaker band at 254 nm, 262 nm and 309 nm can be attributed to ⁸S-⁶D, ⁸S-⁶I and ⁸S-⁶P transition lines of Gd³⁺. The weakest peaks above 300 nm belong to the direct f-f transition lines of Eu³⁺. The presence of the (Y,Gd)₂O₃ host band and Gd³⁺ excitation lines in the excitation spectrum of Eu³⁺ indicates that there exists an energy transfer from the (Y,Gd)₂O₃ host and the Gd³⁺ to the doped Eu³⁺. All the emission lines at 583,

 $587 \sim 599$, 612, 652 and 708 nm are assigned to $^{5}D_{0} - ^{7}F_{J}$ (J = 0, 1, 2, 3, 4) transitions of Eu³⁺, respectively, with $^5D_0 - ^7F_2$ hypersensitive electric dipole transition (612 nm) being the most prominent group, suggesting that Eu³⁺ is located at a site with no inversion symmetry. 42,43 For YGO-Ac* NPs catalyzed by FeCl₃•6H₂O, only by enhancing the excitation voltage can we obtain the similar excitation and emission spectra as YGO-Ac NPs, however, the transition lines of Gd³⁺ are tough to be detected in excitation spectrum and the corresponding emission intensity is lower than that of YGO-Ac NPs. Their luminescence decay curves for the representative emission of Eu³⁺ (612nm, 5D_0 - 7F_2) can be well fitted by a single-exponential function as $I(t) = I_0 e^{-t/\tau}$ (I_0 is the initial emission intensity at t = 0, and τ is the 1/e lifetime of the emission center), the shortened lifetime τ in YGO-Ac* NPs (0.52ms, Figure 2d) with respect to YGO-Ac NPs (1.01 ms, Figure 2c) can be correlated to the decreased emission intensity of Eu³⁺. The luminescence phenomena are in agreement with the wide-angle XRD results (Figure 2e) which demonstrate that YGO-Ac NPs have more detectable crystal faces and better crystallinity than YGO-Ac* NPs.

To realize upconversion emission, phosphors should emit a higher energy photon after absorbing two or more lower energy excitation photons on the basis of sequential absorption and energy-transfer steps. 44 When the doping Eu³⁺ ion in Gd³⁺-based host matrix is replaced with other light-emitting ions that have an absorption band corresponding to the energy of the pumping photons, such as Yb³⁺/Er³⁺, Yb³⁺/Tm³⁺, Yb³⁺/Ho³⁺ ions, they can exhibit characteristic upconversion emissions under lower-energy near-infrared (NIR, 980 nm) excitation. 8 However,

under 800 nm/920 nm Ti:Sapphire femtosecond laser excitation, ultraviolet-absorbing luminophores may become excitable because the pumping photons (two or three photons) are absorbed simultaneously rather than sequentially, thus preventing ultraviolet-induced photodamage and competing with Rayleigh scattering. 22,45 Figure 2f shows that upconversion red fluorescence characteristic of YGO-Ac NPs can be observed in a darkroom by exciting with an 800 nm Ti:Sapphire femtosecond laser and recorded by a digital camera with an 800 nm high reflective mirror in front to eliminate NIR scattering, the corresponding spectrum collected by simple manual detection shows the representative emission of Eu³⁺ (612nm, ⁵D₀-⁷F₂) (inset of Figure 2f).



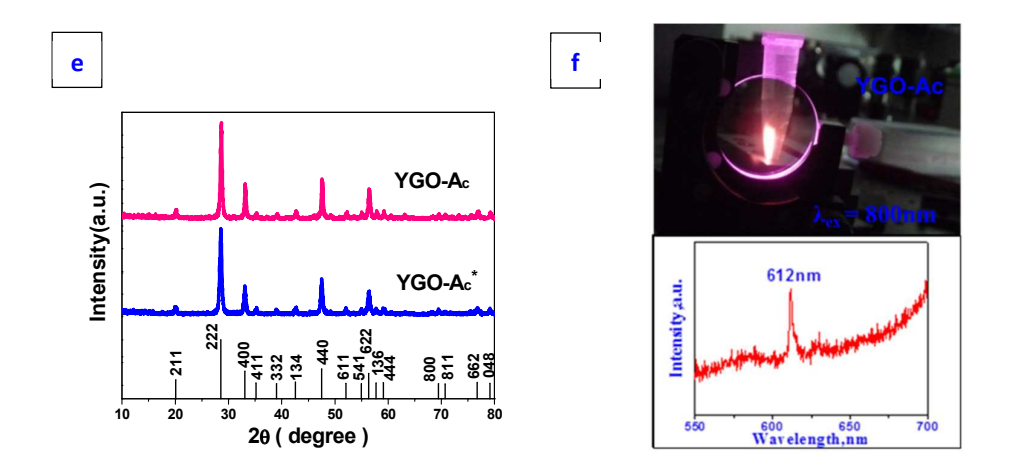


Figure 2. Excitation and emission spectra of (a) YGO-Ac NPs (excitation voltage = 535 V) and (b) YGO-Ac* NPs (excitation voltage = 700 V). Luminescence decay curves for the ${}^5D_0-{}^7F_2$ emission of Eu³⁺ in (c) YGO-Ac and (d) YGO-Ac* NPs. (e) Wide-angle XRD patterns of YGO-Ac and YGO-Ac* NPs, the standard data for Gd₂O₃ (JCPDS card 65-3181) is also presented in the wide-angle XRD patterns for comparison. (f) Photograph and upconversion luminescence spectrum (the inset) of YGO-Ac NPs under 800 nm Ti:Sapphire femtosecond laser excitation.

The room temperature magnetization (M) of YGO-Ac and YGO-Ac* NPs, as a function of applied field (H) (-16 to +16 kOe) shows a linear correlation with the same magnetization value of 2.0 emu/g (at 16 kOe), suggesting that they are paramagnetic and the magnetism is not affected by solvothermal catalyst (Figure 3).

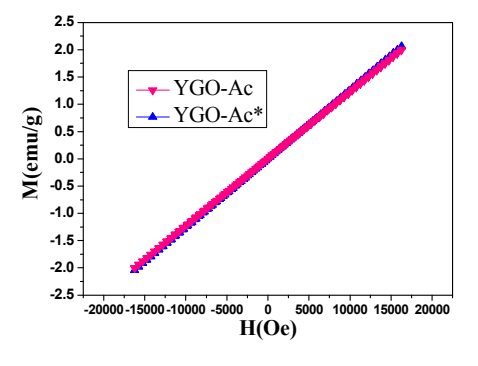


Figure 3. Room temperature magnetization curves of YGO-Ac and YGO-Ac* NPs.

 N_2 adsorption/desorption isotherms of YGO-Ac (Figure 4a) and YGO-Ac* NPs (Figure 4b) exhibit typical IV-typed curves with H_1 -hysteresis loops, indicating their mesopore systems. The BET surface area and total pore volume are calculated to be $24/9 \text{ m}^2\text{g}^{-1}$ and $0.12/0.06 \text{ cm}^3\text{g}^{-1}$ respectively (Table 2), their mesopore size distribution curves (inset of Figure 4) exhibit peaks centered at the mean value of 20.1/27.5 nm. Given the FWHM (the full width at half maximum) is quite large, we speculate that the mesoporous structure may mainly originate from the stacking of spherical NPs, they may pack into three-dimensional ordered arrays under magnetic guidance from Gd^{3+} (Figure 1a). In addition, the mesoporous structure may also result from the removal of co-surfactant by calcination.

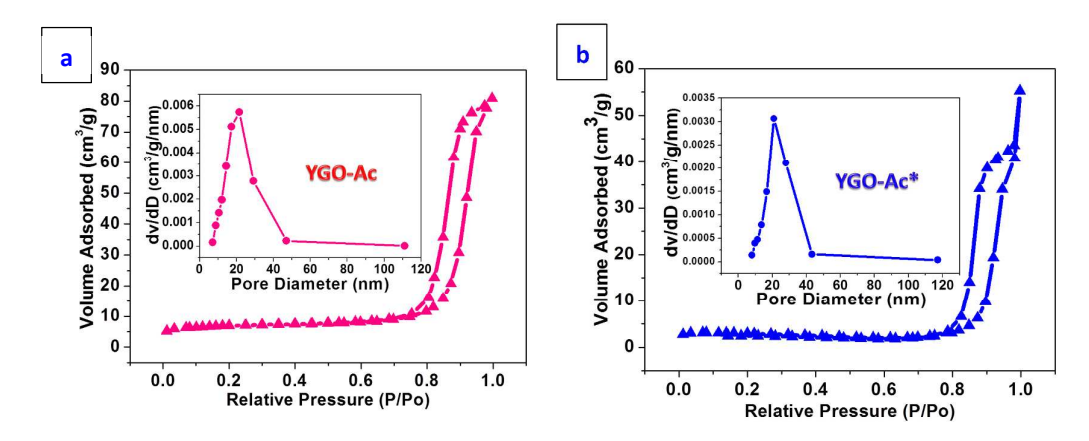


Figure 4. N₂ adsorption/desorption isotherms and mesopore size distribution curves (the inset) of (a) YGO-Ac and (b) YGO-Ac* NPs.

Table 2. Mesoporous parameters for core and core-shell NPs.

Sample	YGO-Ac	YGO-Ac*	YGO-Bmc	YGO-Bmc ^{8:1}	YGO-Bmnc
S _{BET} (m ² /g)	24	9	299	184	562
Vp(cm ³ /g)	0.12	0.06	0.16	0.12	0.37
Dp(nm)	20.1	27.5	< 2.0	<2.0	2.6

From these comparison, we come to conclusions that: 1) Solvothermal process catalyzed by conc. HNO₃ is homogeneous while by FeCl₃•6H₂O is heterogeneous, thus resulting in the NPs with different colors which in turn have a crucial impact on the fluorescence intensity of NPs, because the shallower the color of phosphor is, the weaker the effect of light scattering will be, and the better the corresponding fluorescence intensity and color purity of the phosphor will be. 2) Compared with heterogeneous catalysis, homogeneous catalysis is more beneficial for crystallization, because homogeneous catalysis can prompt more Eu³⁺ (discrete luminescence center) to occupy the low symmetrical site of (Y,Gd)₂O₃ host to enhance the efficiency of energy transfer, resulting in NPs with better crystallinity, fluorescence intensity and mesoporous properties. 3) The magnetization of NPs is only associated with the dislodgement of co-surfactant and the transformation of amorphous Gd(OH)₃ into crystal Gd₂O₃.

3.3. Regulation of Mesoporous property for YGO-Bmnc NPs. Through two-step sol-gel process, a typical sandwich structure with a hydrophilic core, a nonporous silica layer in the middle layer, and mesoporous silica phase in the outer layer was successfully fabricated. Notably, the cylindrical silica channels of YGO-Bm NPs are clearly found to be perpendicular to the spheres' surface while the silica mesopores of YGO-Bm^{8:1} NPs are still random (Figure 5). The low-angle XRD pattern of YGO-Bmc NPs shows a strong (100) peak at $2\theta = 2.4^{\circ}$ which reveals an ordered 2D mesopore symmetry while no apparent peak is found for YGO-Bmc^{8:1} NPs (Figure S2c, d).

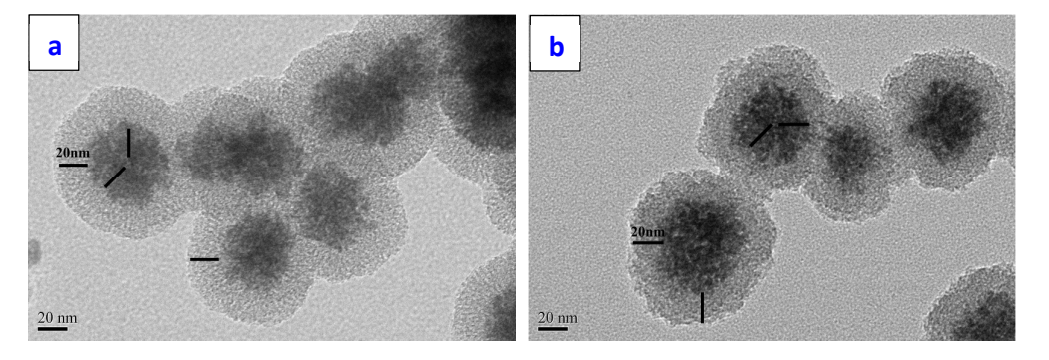


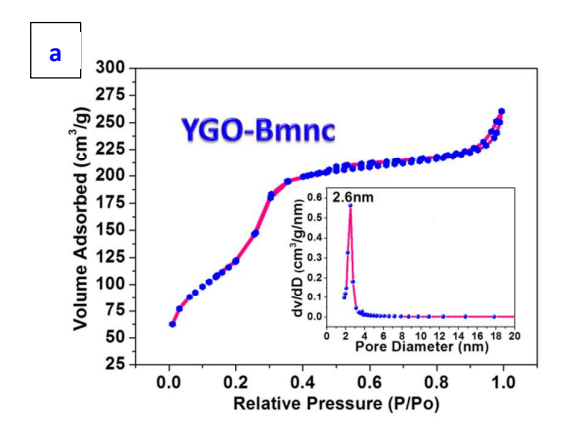
Figure 5. TEM images of (a) YGO-Bm NPs and (b) YGO-Bm^{8:1} NPs.

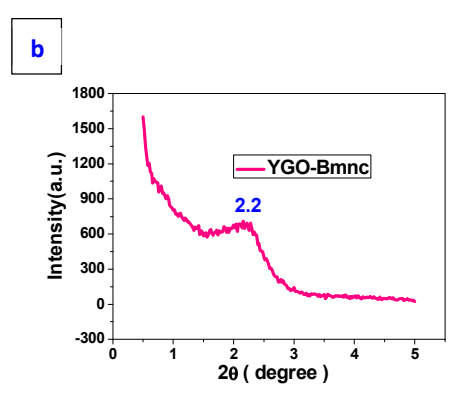
The surfactant-assistant sol-gel silica coating process can be divided into three stages: first stage, co-assembly of silica oligomers and CTAB templates into silicate/CTA⁺ complexes driven by coulombic 46 forces or hydrogen bonding 47 interactions; second stage, the deposition of silicate/CTA⁺ complexes on the surface of hydrophilic nanocore; third stage, the optimization of mesoporous structure. Obviously, the second stage is a kind of watershed in constructing of perpendicularly aligned mesoporous silica shell, because in ethanol/water mixture, ethanol acts as cosolvent and its low-dielectric constant can significantly reduce the polarity and the surface tension of the system, which in turn has two sides on micelle organization and particle morphology. 48 As the amount of ethanol increasing, on the one hand, the specific surface energy of silicate or silicate/CTA⁺ complexes will be reduced, thus preventing these complexes from homogeneous nucleating and spontaneously aggregating into core-free silica NPs; on the other hand, the critical micelle concentration (CMC) of CTAB will be increased accordingly, the size of the micelles and their numbers will be decreased, thus destroying the long-range ordering of micelles, 49 making mesoporous structure random and disordered. Consequently, in the first silica coating step (formation of nonporous silica layer), the volume ratio of

ethanol and water must be kept at 8:1 to ensure one-to-one coating without core-free silica particles; in the second step (formation of mesoporous silica layer), because of the affinity between nanocore and silicate/CTA⁺ complexes enhanced by the nonporous silica layer forming in the first step, the volume ratio of ethanol and water can be reduced to 3:4 to guarantee the good coating morphology and construct perpendicularly aligned mesoporous silica shell. Interestingly, the preferable perpendicularly alignment fashion of silicate/CTA⁺ complexes on the nonporous silica layer probably result from the attraction between polar and nonpolar species happens to be equal when the volume ratio of ethanol to water is 3:4. In addition, a control test was also made, 50 the hydrolysis and condensation of TEOS were carried out directly in ethanol/water mixture (volume ratio = 3:4, containing CTAB templates and be prealkalized to pH 9~10 with ammonia solution). Then it could be investigated that mesoporous silica nanospheres (mSiO₂) were successfully obtained, their ordered mesochannels radiated out from the center (Figure S3). This phenomenon further confirms the perpendicularly aligned mesoporous silica coating mechanism discussed above.

As an added bonus, we can endow sandwich-like NPs better mesoporous structure, higher BET surface area and bigger mesopore volume via a highly simple, efficient, mild ion-exchange method (NH₄NO₃/EtOH) to pre-process CTAB templates before calcination. N₂ adsorption/desorption isotherms of YGO-Bmnc NPs (Figure 6a) display typical IV-typed curves with H₁-hysteresis loops, the BET surface area and total pore volume are calculated to be 562 m²g⁻¹ and 0.37 cm³g⁻¹ respectively, and the

mesopore size distribution curve exhibits a sharp peak centered at the mean value of 2.6 nm, superior to YGO-Bmc NPs and YGO-Bmc^{8:1} NPs (Figure S2a~b and Table 2). The low-angle XRD pattern of YGO-Bmnc NPs (Figure 6b) shows a strong (100) peak at $2\theta = 2.2^{\circ}$ which is slightly left-shifted compared with YGO-Bmc NPs (Figure S2c), corresponding to the expansion of mesopore volume. All these results testify that pre-process CTAB templates with NH₄NO₃/EtOH mixture before calcination can guarantee complete removal of templates without corroding the nanocore (Figure 6c and Figure S4) and prevent the mesopore structure from being damaged in calcination process. DLS measurement (Figure 6d) reveals that the hydrodynamic size of YGO-Bmnc NPs is 105 nm. The basic principle is that, NH₄⁺ in NH₄NO₃/EtOH solution can take place of the heads groups of surfactant molecules (CTA⁺) due to their chemical and geometrical similarities, and the NH₄⁺ will be transformed into NH₃ by heating at moderate temperature, 40 thus keeping the mesoporous structure in position. Compared with other extraction methods, it is more simple and efficient than acetone extraction method³¹ which takes as long as 48 h; it is milder than acidic ethanol (HCl/EtOH) extraction method ^{17,28} which may cause core-free silica NPs.





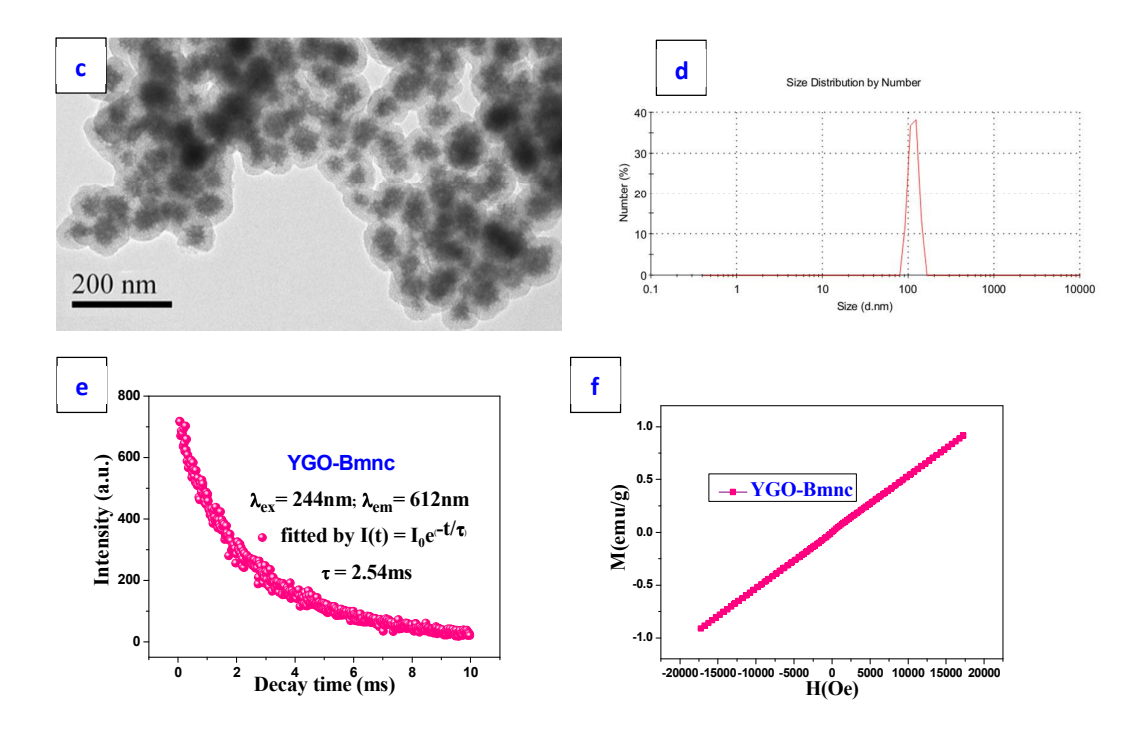


Figure 6. (a) N₂ adsorption/desorption isotherms and mesopore size distribution curve (the inset), (b) low-angle XRD pattern, (c) TEM image, (d) DLS size distribution (in normal saline), (e) luminescence decay curve, (f) room temperature magnetization curve of YGO-Bmnc NPs.

3.4. Luminescence and Magnetic Properties of YGO-Bmnc NPs. The luminescence decay curve of YGO-Bmnc NPs for the representative emission of Eu³⁺ (612nm, 5D_0 - 7F_2) can be well fitted by a single-exponential function (Figure 6e). The prolonged lifetime in YGO-Bmnc NPs (2.54 ms) with respect to YGO-Ac nanocore (1.01 ms) can be attributed to the decreased effective refractive index (the refractive index of Gd_2O_3 and SiO_2 are 1.8 and 1.45, respectively⁵¹).

The room temperature magnetization curve of YGO-Bmnc NPs demonstrates that the core-shell NPs preserve the paramagnetic character of YGO-Ac nanocore, but the magnetization value decreased to 0.85 emu/g (at 16 kOe) after coating (Figure 6f).

3.5. Cytotoxicity Assay and Optical-MR Dual-Modal Imaging. MTT assay shows good biocompatibility of YGO-Bmnc NPs to cancer and normal cells, the IC₅₀ (the concentration of NPs that inhibited 50% of cell growth) ([Gd]) obtained for each cell type is above 1000 μg/mL (6.36 mM) even after 72 h incubation (Figure S5).

Cellular uptake of YGO-Bmnc NPs was verified by inverted fluorescence microscope following the incubation of BxPC-3 cells with NPs for 48 h (Figure 7a~b). Blue fluorescence of DAPI was observed in the nucleus and red fluorescence of YGO-Bmnc NPs was found in the cytoplasm under WU (330~385 nm) excitation (Figure 7b), clearly demonstrating that YGO-Bmnc NPs are good candidates as fluorescently-labeled probes.

To examine the feasibility of using YGO-Bmnc NPs as T_1 MRI contrast agent, the relaxation time of YGO-Bmnc NPs was measured on a 3.0 T clinical MRI scanner. As [Gd] increased, we can see signal enhancing in T_1 -weighted images and signal receding in T_2 -weighted images (Figure 7c). The r_1 and r_2 relaxivities of YGO-Bmnc NPs were 5.05 mM⁻¹s⁻¹ and 6.14 mM⁻¹s⁻¹ respectively (Figure 7d). The r_2/r_1 ratio is an important parameter to estimate the efficiency of T_1 contrast agents, it closely relates to the properties of NPs as well as field strengths, because for the same NPs, lower field gave higher r_1 but similar r_2 values and the r_2/r_1 ratio is lower accordingly.^{25,52,53} "Magnevist", a commercial gadolinium complex, has an optimal r_2/r_1 ratio of 1.0 (r_1 = 4.6 mM⁻¹s⁻¹, r_2 = 4.5 mM⁻¹s⁻¹) at 1.5 T_1 , by that analogy, the r_2/r_1 ratio at 3.0 T will be above 1.0. No matter how strong the field strength can be, T_1 agents usually have r_2/r_1 ratios of 1-2, whereas that value for T_2 agents, such as iron oxide particles, is as

high as 10 or more.⁵⁵ The r_2/r_1 ratio of YGO-Bmnc NPs was 1.216 at 3.0 T similar to "Magnevist", demonstrating that YGO-Bmnc NPs can be efficient T_1 contrast agents. All these results point to the potential application of YGO-Bmnc NPs as a dual-function imaging probe for simultaneous optical-MR dual-modal imaging.

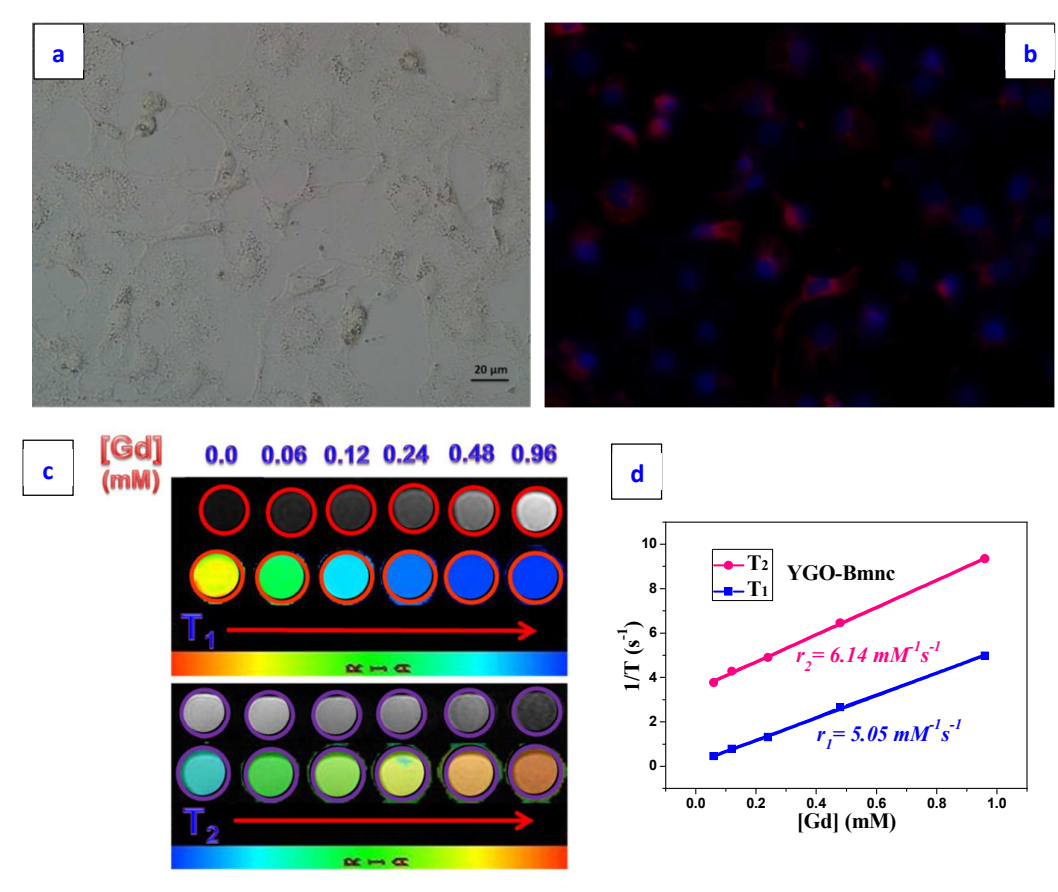


Figure 7. Inverted fluorescence microscopic images of BxPC-3 cells incubated with YGO-Bmnc NPs for 48 h (the nuclei stained with DAPI): (a) bright-field, (b) under WU (330~385 nm) excitation; (c) T₁ and T₂-weighted MR images and color maps of YGO-Bmnc NPs at various [Gd], (d) plot of 1/T (s⁻¹) versus [Gd] (mM).

4. Conclusions

In summary, we have synthesized and characterized a new kind of Gd³⁺-based multifunctional nanomedical platform with particle size smaller than 200 nm and specific surface area larger than 500 m²g⁻¹ for combined multimodal diagnosis and therapy. The fluorescence characteristic, paramagnetic behavior and mesoporous structure are fully discussed. 40 nm-sized (Y,Gd)₂O₃:Eu³⁺ (YGO-Ac) nanocore is synthesized by a one-pot solvothermal method, which is highly efficient and environmental friendly. The size of YGO-Ac NPs mainly depends on the ratio of co-surfactant whereas their properties are significantly affected by the kinds of catalyst. Through two-step sol-gel process, coating of 20 nm-sized perpendicularly aligned mesoporous silica shell onto hydrophilic NPs is successfully achieved without core-free silica NPs, the surface area can be increased from 24 m²/g (YGO-Ac nanocore) to 299 m²/g (YGO-Bmc core-shell NPs), even to 562 m²/g (YGO-Bmnc core-shell NPs) with the introduction of a highly efficient surfactant removal method (NH₄NO₃/EtOH). These YGO-Bmnc NPs are nontoxic and show good performance in optical imaging and T_1 -weighted MRI. Most importantly, their r_2/r_1 ratio (r_1 = 5.05) $\text{mM}^{-1}\text{s}^{-1}$, $r_2/r_1=1.216$, at 3.0T) in T_1 -weighted MRI is much lower than other existing Gd³⁺-based nanoscale contrast agents. Along with their highly ordered mesoporous structure (S_{BET} : $562m^2/g$, Vp: $0.37cm^3/g$, Dp: 2. 6nm), they can not only load other imaging agents to fulfill multimodal imaging, but also monitor drug/nucleic acid/protein loading by means of imaging. All of these features make them have a great potential for combined multimodal diagnosis and therapy.

Acknowledgements

This work was supported by the National Natural Science Foundation of China (No. 21373138), National 973 Project (2010CB933901), Shanghai Sci. & Tech. Committee (12JC1407200), Program for Changjiang Scholars and Innovative Research Team in University (IRT1269).

Notes and references

- 1 A. Burns, H. Ow and U. Wiesner, Chem. Soc. Rev., 2006, 35, 1028-1042.
- 2 J. Kim, Y. Piao, and T. Hyeon, Chem. Soc. Rev., 2009, 38, 372-390.
- 3 L. E. Jennings, and N. J. Long, Chem. Commun., 2009, 3511-3524.
- 4 J. E. Lee, D. J. Lee, N. Lee, B. H. Kim, S. H. Choi, and T. Hyeon, *J. Mater. Chem.*, 2011, **21**, 16869-16872.
- 5 M. Colombo, S. Carregal-Romero, M. F. Casula, L. Gutiérrez, M. P. Morales, I. B. Böhm, J. T. Heverhagen, D. Prosperi, and W. J. Parak, *Chem. Soc. Rev.*, 2012, 41, 4306-4334.
- 6 W. Di, X. Ren, H. Zhao, N. Shirahata, Y. Sakka, and W. Qin, *Biomaterials*, 2011, 32, 7226-7233.
- 7 G. K. Das, B. C. Heng, S. Ng, T. White, J. S. C. Loo, L. D'Silva, P. Padmanabhan, K. K. Bhakoo, S. T. Selvan, and T. T. Y. Tan, *Langmuir*, 2010, 26, 8959-8965.
- 8 S. Gai, P. Yang, D. Wang, C. Li, N. Niu, F. He, and X. Li, *CrystEngComm*, 2011, **13**, 5480-5487.
- 9 T. Paik, T. R. Gordon, A. M. Prantner, H. Yun, and C. B. Murray, ACS Nano, 2013, 7, 2850-2859.
- 10 S. Rodriguez-Liviano, N. Nuñez, S. Rivera-Fernández, J. Fuente, and M. Ocaña, *Langmuir*, 2013, 29, 3411-3418.
- 11 R. M. Petoral, J. F. Söderlind, A. Klasson, A. Suska, M. A. Fortin, N. Abrikossova, L. Selegård, P. Käll, M. Engström, and K. Uvdal, *J. Phys. Chem. C*, 2009, **113**, 6913-6920.

- 12 N. Johnson, W. Oakden, G. Stanisz, R. Prosser, and F. Veggel, *Chem. Mater.*, 2011, 23, 3714-3722.
- 13 G. Tian, Z. Gu, X. Liu, L. Zhou, W. Yin, L. Yan, S. Jin, W. Ren, G. Xing, S. Li, and Y. Zhao, J. Phys. Chem. C, 2011, 115, 23790-23796.
- 14 L. Zhou, Z. Gu, X. Liu, W. Yin, G. Tian, L. Yan, S. Jin, W. Ren, G. Xing, W. Li, X. Chang, Z. Hu, and Y. Zhao, *J. Mater. Chem.*, 2012, 22, 966-974.
- Z. Liu, X. Liu, Q. Yuan, K. Dong, L. Jiang, Z. Li, J. Ren, and X. Qu, J. Mater. Chem., 2012,
 14982-14990.
- 16 J. W. M. Bulte, and D. L. Kraitch-man, NMR Biomed., 2004, 17, 484-499.
- 17 J. Kim, H. S. Kim, N. Lee, T. Kim, H. Kim, T. Yu, I. C. Song, W. K. Moon, and T. Hyeon, Angew. Chem. Int. Ed., 2008, 47, 8438-8441.
- 18 M. Liong, J. Lu, M. Kovochich, T. Xia, S. G. Ruehm, A. E. Nel, F. Tamanoi, and J. I. Zink, ACS Nano, 2008, 2, 889-896.
- 19 J. Yang, Y. Deng, Q. Wu, J. Zhou, H. Bao, Q. Li, F. Zhang, F. Li, B. Tu, and D. Zhao, Langmuir, 2010, 26, 8850-8856.
- 20 J. Liu, S. Z. Qiao, Q. H. Hu, and G. Q. Lu, Small, 2011, 7, 425-443.
- 21 J. Zhang, J. M. Rosenholm, and H. Gu, Chemphyschem, 2012, 13, 2016-2019.
- 22 Q. Lü, A. Li, F. Guo, L. Sun, and L. Zhao, Nanotechnology, 2008, 19, 205704.
- 23 J. S. Kim, W. J. Rieter, K. M. L. Taylor, H. An, W. Lin, and W. Lin, J. Am. Chem. Soc., 2007, 129, 8962-8963.
- 24 K. M. L. Taylor, J. S. Kim, W. J. Rieter, H. An, W. Lin, and W. Lin, *J. Am. Chem. Soc.*, 2008, 130, 2154-2155.
- 25 T. Kim, E. Momin, J. Choi, K. Yuan, H. Zaidi, J. Kim, M. Park, N. Lee, M. T. McMahon, A. Quinones-Hinojosa, J. W. Bulte, T. Hyeon, and A. A. Gilad, *J. Am. Chem. Soc.*, 2011, **133**, 2955-2961.
- 26 J. Park, K. An, Y. Hwang, J. G. Park, H. J. Noh, J. Y. Kim, J. H. Park, N. M. Hwang, and T. Hyeon, *Nat. Mater.*, 2004, 3, 891-895.

- 27 K. An, M. Park, J. H. Yu, H. B. Na, N. Lee, J. Park, S. H. Choi, I. C. Song, W. K. Moon, and T. Hyeon, *Eur. J. Inorg. Chem.*, 2012, 2148-2155.
- 28 D. K. Yi, S. S. Lee, G. C. Papaefthymiou, and J. Y. Ying, Chem. Mater., 2006, 18, 614-619.
- 29 J. Kim, J. E. Lee, J. Lee, J. H. Yu, B. C. Kim, K. An, Y. Hwang, C. H. Shin, J. G. Park, J. Kim, and T. Hyeon, *J. Am. Chem. Soc.*, 2006, 128, 688-689.
- 30 T. Suteewong, H. Sai, J. Lee, M. Bradbury, T. Hyeon, S. M. Gruner, and U. Wiesner, *J. Mater. Chem.*, 2010, **20**, 7807-7814.
- 31 Y. Deng, D. Qi, C. Deng, X. Zhang, and D. Zhao, J. Am. Chem. Soc., 2008, 130, 28-29.
- 32 Z. Xu, Y. Gao, S. Huang, P. Ma, J. Lin, and J. Fang, Dalton Trans., 2011, 40, 4846-4854.
- 33 Z. Xu, C. Li, P. Ma, Z. Hou, D. Yang, X. Kang, and J. Lin, *Nanoscale*, 2011, 3, 661-667.
- 34 G. Storm, S. O. Belliot, T. Daemen, and D. D. Lasic, Adv. Drug Deliver Rev., 1995, 17, 31-48.
- 35 M. Gaumet, A. Vargas, R. Gurny, and F. Delie, Eur. J. Pharm. Biopharm., 2008, 69, 1-9.
- 36 M. Yin, M. Wang, F. Miao, Y. Ji, Z. Tian, H. Shen, and N. Jia, Carbon, 2012, 50, 2162-2170.
- 37 X. Hu, Y. Ji, M. Wang, F. Miao, H. Ma, H. Shen, and N. Jia, *J. Biomed. Nanotechnol.*, 2013, 9, 976-984.
- 38 Y. Wang, X. Bai, T. Liu, B. Dong, L. Xu, Q. Liu, and H. Song, *J. Solid State Chem.*, 2010, **183**, 2779-2785.
- 39 J. Zhang, X. Li, J. M. Rosenholm, and H. Gu, J. Colloid Interface Sci., 2011, 361, 16-24.
- 40 N. Lang, and A. Tuel, Chem. Mater., 2004, 16, 1961-1966.
- 41 K. X. Yao, and H. C. Zeng, J. Phys. Chem. C, 2007, 111, 13301-13308.
- 42 J. Yang, C. Li, Z. Cheng, X. Zhang, Z Quan, C. Zhang, and J. Lin, *J. Phys. Chem. C*, 2007, **111**, 18148-18154.
- 43 L. Hu, R. Ma, T. C. Ozawa, and T. Sasaki, Angew. Chem. Int. Ed., 2009, 48, 3846-3849.
- 44 A. C. Tropper, J. N. Carter, R. D. T. Lauder, D. C. Hanna, S. T. Davey, and D. Szebesta, J. Opt. Soc. Am. B, 1994, 11, 886-893.
- 45 J. H. Yu, S. Kwon, Z. Petrášek, O. K. Park, S. W. Jun, K. Shin, M. Choi, Y. I. Park, K. Park, H. B. Na, N. Lee, D. W. Lee, J. H. Kim, P. Schwille, and T. Hyeon, *Nat. Mater.*, 2013, 12, 359-366.

- 46 Q. Huo, D. I. Margolese, U. Ciesla, P. Feng, T. E. Gier, P. Sieger, R. Leon, P. M. Petroff, F. Schüth, and G. D. Stucky, *Nature*, 1994, **368**, 317-321.
- 47 P. T. Tanev, and T. J. Pinnavaia, Science, 1995, 267, 865-867.
- 48 B. Tan, and S. E. Rankin, J. Phys. Chem. B, 2004, 108, 20122-20129.
- 49 K. Fontell, A. Khan, B. Linström, D. Maciejewska, and S. Puang-Ngern, *Colloid Polym. Sci.*, 1991, **269**, 727-742.
- 50 H. Cao, X. Hu, C. Hu, Y. Zhang, and N. Jia, Biosens. Bioelectron., 2013, 41, 911-915.
- 51 T. Liu, Y. Wang, H. Qin, X. Bai, B. Dong, L. Sun, and H. Song, *Mater. Res. Bull.*, 2011, 46, 2296-2303.
- 52 H. B. Na, I. C. Song, and T. Hyeon, Adv. Mater., 2009, 21, 2133-2148.
- 53 B. H. Kim, N. Lee, H. Kim, K. An, Y. I. Park, Y. Choi, K. Shin, Y. Lee, S. G. Kwon, H. B. Na, J. G. Park, T. Y. Ahn, Y. W. Kim, W. K. Moon, S. H. Choi, and T. Hyeon, *J. Am. Chem. Soc.*, 2011, 133, 12624-12631.
- 54 W. S. Seo, J. H. Lee, X. Sun, Y. Suzuki, D. Mann, Z. Liu, M. Terashima, P. C. Yang, M. V. McConnell, D. G. Nishimura, and H. Dai, *Nat. Mater.*, 2006, 5, 971-976.
- 55 P. Caravan, J. J. Ellison, T. J. McMurry, and R. B. Lauffer, *Chem. Rev.*, 1999, **99**, 2293-2352.